# Physico-Chemical Investigation of the Panchromatic Effect on β-Substituted ZnII Porphyrinates for DSSCs: The Role of the π Bridge between a Dithienylethylene Unit and the Porphyrin...

**ARTICLE** *in* THE JOURNAL OF PHYSICAL CHEMISTRY C · APRIL 2014

Impact Factor: 4.77 · DOI: 10.1021/jp412087f

THE JOURNAL OF PHYSICAL CHEMISTRY C

Article

pubs.acs.org/JPCC

# Physicochemical Investigation of the Panchromatic Effect on β-Substituted Zn$^{II}$ Porphyrinates for DSSCs: The Role of the π Bridge between a Dithienylethylene Unit and the Porphyrinic Ring

Gabriele Di Carlo,[†] Alessio Orbelli Biroli,[‡] Francesca Tessore,[†] Maddalena Pizzotti,*[,†] Patrizia Romana Mussini,[†] Anna Amat,[∥] Filippo De Angelis,[∥] Alessandro Abbotto,[§] Vanira Trifiletti,[§] and Riccardo Ruffo[§]

[†]Dipartimento di Chimica, dell'Università degli Studi di Milano, Unità di Ricerca dell'INSTM, via C. Golgi 19, 20133 Milano, Milano, Italy

[‡]Istituto di Scienze e Tecnologie Molecolari del CNR (CNR-ISTM), via C. Golgi 19, 20133 Milano, Milano, Italy

[§]Department of Materials Science and Solar Energy Research Center MIB-SOLAR, and INSTM Unit, University of Milano Bicocca, Via Cozzi 55, I-20125 Milano, Milano, Italy

[∥]Computational Laboratory for Hybrid/Organic Photovoltaics (CLHYO), Istituto di Scienze e Tecnologie Molecolari del CNR (CNR-ISTM), Via Elce di Sotto 8, 06123 Perugia, Perugia, Italy

Supporting Information

**ABSTRACT:** Three novel dyes based on Zn$^{II}$ porphyrinates combined, in β-pyrrolic position, with the π unit dithienylethylene (DTE) have been synthesized and investigated for application in DSSCs. The panchromatic effect due to elongation of the π-delocalized system through a bridge between the porphyrinic ring and the DTE unit such as the 4-ethynylstyryl (**1**), ethynyl (**2**), and ethenyl (**3**) bonds have been investigated by computational, electrochemical, and photoelectrochemical methods. For all three dyes the π conjugated substituents in the β position produced the expected panchromatic effect with broadened electronic absorption spectra over a wide range of wavelengths and IPCE spectra featuring a broad plateau in the region 430−650 nm. In addition both DFT computational and electrochemical data have shown a smaller HOMO−LUMO energy gap for dye **3**, when compared to dye **2** suggesting a slightly more facile conjugation between the porphyrinic core and the DTE unit through the ethenylic bond. Conversely the photoelectrochemical investigation showed improved DSSC performances from **3** to **1**. These results have been rationalized by an in-depth DFT computational study of dyes **2** and **3** interacting with a cluster of 82 $TiO_2$ units. The small energetic overlap between the LUMO and the $TiO_2$ conduction band characterizing the more structurally distorted dye **3** would suggest low quantum yield of electron injection, while dye **2** shows a greater interaction between the LUMO of the dye and the semiconductor. Consequently the increased linearity and planarity of the structure of dye **1** seems to be the origin of its best performance in DSSC. Therefore it appears that the nature of the bridge between the DTE unit and the porphyrinic ring is quite relevant for the efficiency of these dyes for DSSC, due to distortion from the planarity and linearity of the structure of the dye and the consequent changes on the dye π conjugation.

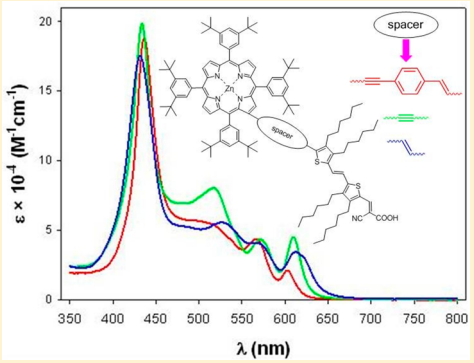


## INTRODUCTION

Dye sensitized solar cells (DSSCs) are attractive alternative to conventional solar cells due to their relatively low cost since O'Regan and Gratzel's pioneering work.[1] An ideal molecular sensitizer (dye) for DSSC requires an electronic spectrum with bands characterized by large absorption coefficients and a broad spectral coverage up to the near-infrared region as well as good chemical and photochemical stability.[2]

In the photosynthetic cores of bacteria and plants, solar energy is collected at chromophores based on porphyrinic structures,[3] and the captured energy is converted to chemical energy by complex biological redox processes. Inspired by this natural process of light harvesting and conversion, numerous porphyrins have been investigated as dyes for DSSC.[4] The intrinsic advantages of porphyrinic dyes are their high chemical and photochemical stability and their very strong Soret (about 450 nm), and strong Q (550−650 nm), absorption bands. In addition their electrochemical and light harvesting properties are tunable acting on four *meso* and eight β pyrrolic positions, by specific chemical functionalization. The energy level of the lowest unoccupied molecular orbital (LUMO) of metal porphyrins is generally above the energy of the $TiO_2$

**Received:** December 10, 2013
**Revised:** March 18, 2014
**Published:** March 20, 2014

  

conduction band allowing efficient electron injection, while the energy of the highest occupied molecular orbital (HOMO) is below the redox potential of today's most used electrolyte ($I^-/I_3^-$) for efficient dye regeneration.[2]

In particular *meso* disubstituted push−pull $Zn^{II}$ porphyrinates, characterized by a strong and directional electron excitation process along the push−pull system, have been extensively investigated as dyes for DSSCs.[4] Nowadays the highest solar cell efficiency ($\eta$ = 12.3%) is reached by a well engineered *meso* disubstituted push−pull $Zn^{II}$ porphyrinate, cosensitized with an organic dye, using a cobalt based electrolyte.[5] Even though *meso* disubstituted push−pull $Zn^{II}$ porphyrinates dyes are often featured by interesting light conversion efficiencies,[4] multistep synthetic procedures are required, characterized by very low overall yields.[6,7] Recently we took advantage of a microwave-assisted synthetic approach to successfully obtain $\beta$ mono- or disubstituted push−pull $Zn^{II}$ porphyrinates in a few steps.[8] Furthermore we have shown that $\beta$ mono- or disubstituted push−pull $Zn^{II}$ porphyrinic dyes show comparable or improved efficiency as sensitizers in DSSC, despite a higher HOMO−LUMO energy gap compared to *meso* disubstituted $Zn^{II}$ porphyrinic dyes.

IPCE (Incident Photon-to-Current Efficiency) spectra of $Zn^{II}$ porphyrinic dyes generally show two well separated absorption peaks corresponding to B and Q absorption bands, with a region of lower intensity between 450 and 550 nm. IPCE spectra with a significant intensity over a broad range of wavelengths may be achieved by two means:

i) addition of an organic cosensitizer with significant electronic absorption (IPCE intensities between 430 and 600 nm[5]) to the porphyrinic dye; ii) introduction of an (*E*)-dithienylethylene (DTE) unit in a $\pi$ delocalized chain connecting the porphyrinic ring and the carboxylic anchoring group, as reported by Bisquert, Langa et al.[9] in order to produce a relevant electronic absorption between 430 and 650 nm and significant IPCE intensities in this region.

Furthermore it was also shown that the attachment of thienyl units induces a bathochromic shift of the electronic absorption bands, with an enhancement of their intensity together with an increased lifetime of the excited state.[9,10]

We have thus applied this latter panchromatic strategy when such kind of $\pi$ delocalized thienylic chain, carrying the cyanoacrylic anchoring group and a DTE unit, is linked to the $\beta$ position of the porphyrinic ring. Hereafter we report the synthesis, electrochemical, and theoretical investigation of a series of $\beta$ substituted $Zn^{II}$ porphyrinates carrying a cyanoacrylic anchoring group connected to the $\beta$ position through an ethynyl or ethenyl or 4-ethynylstyryl group linked to a DTE unit, together with the comparative evaluation of their performance as dyes in DSSCs.

## EXPERIMENTAL SECTION

All reagents and solvents used in the synthesis were purchased from Sigma Aldrich and used as received, except $Et_3N$, $Et_2NH$ (freshly distilled over KOH), and THF (freshly distilled from Na/benzophenone under nitrogen atmosphere). Silica gel for gravimetric chromatography (Geduran Si 60, 63−200 $\mu$m) and for flash chromatography (Geduran Si 60, 40−63 $\mu$m) were purchased from Merck.

Glassware was flame-dried under vacuum before use when necessary.

(*E*)-5-(2-(3,4-Dihexylthiophen-2-yl)vinyl)-3,4-dihexylthiophene-2-carbaldehyde (**13**),[9,11,12] (*E*)-(5-(2-(3,4-dihexylthiophen-2-yl)vinyl)-3,4-dihexylthiophen-2-yl)methanol (**15**),[11] (*E*)-diethyl((5-(2-(3,4-dihexylthiophen-2-yl)vinyl)-3,4-dihexylthiophen-2-yl)methyl)phosphonate (**16**),[11] [2-(4-carboxyaldehyde-phenylethynyl)-5,10,15,20-tetrakis(3,5-di-*tert*-butylphenyl)porphyrinate] Zn(II) (**4**),[8] and [2-formyl-5,10,15,20-tetrakis(3,5-di-*tert*-butylphenyl)porphyrinate]Zn(II) (**10**)[13] were prepared as reported in the literature.

$^1$H NMR spectra were recorded on a Bruker Avance DRX-400 and on a Bruker AMX 300 in $CDCl_3$ as solvent with addition, when necessary, of a drop of pyridine-$d_5$ or in THF-$d_8$ (Cambridge Isotope Laboratories, Inc.). Electronic absorption spectra were recorded using a Jasco V-530 spectrometer; the emission spectra were recorded using a Jobin-Yvon Fluorolog-3 spectrometer equipped with double monochromators and Hamamatsu-928 photomultiplier tube (PMT) as the detector. Mass spectra were obtained with a VG Autospec M246 magnetic mass spectrometer with an LSIMS ionic source. Microwave-assisted reactions were performed using a Milestone MicroSYNTH instrument.

## COMPUTATIONAL METHODOLOGY

DFT (Density Functional Theory) and TDDFT (Time Dependent Density Functional Theory) calculations were performed for all the investigated $Zn^{II}$ porphyrinates using the Gaussian 09 program package.[14] To reduce the computational overhead, the *tert*-butyl aryl substituents were replaced by hydrogen atoms. The molecular structures were fully optimized *in vacuo* using the B3LYP[15] functional and a 6-311g* basis set.[16] On the optimized structures, we performed single point calculations including solvation effects (THF) by means of a conductor-like polarizable continuum model (CPCM),[17] to compute the energies and electron density distribution of the relevant occupied/unoccupied molecular orbitals. The absorption spectra were simulated in THF solution by computing the lowest 20 singlet−singlet excitation energies; the computed spectra were analyzed in terms of the molecular orbital composition of the main transitions. Moreover, to check the performance of the B3LYP functional these systems, TD calculations using CAM-B3LYP[18] were also performed.

In addition, in order to compare the energy of computed and experimental electrochemical HOMO and LUMO levels, for dye **3** we have explicitly calculated the so-called ground state potential (GSOP) and the excited state oxidation potentials (ESOP) following a theoretical methodology developed by some of us.[19,36] The GSOP was computed as the free energy difference between neutral and oxidized dyes in their ground state optimized structures. The ESOP is the energy difference between the neutral and the oxidized species on the first excited state at their optimized structures and can be estimated by computing the ESOP as

$$\mathrm{ESOP} \simeq \mathrm{GSOP} - E_{0-0}$$

where $E_{0-0}$ is the adiabatic lowest excitation energy. We have approximated the $E_{0-0}$ by the lowest transition, neglecting the geometry and energy reorganization on the excited state.

To gain insight on the electronic effects promoted by the interactions between the $Zn^{II}$ porphyrinates and the $TiO_2$ semiconductor, we have modeled a $TiO_2$ surface using a stoichiometric anatase cluster of 82 $TiO_2$ units exposing the (101) surface, a theoretical approach developed and already applied by some of us.[8,19,20] On the semiconductor cluster the optimized dye structure was anchored in a bidentate mode, and a single point calculation was performed.


dx.doi.org/10.1021/jp412087f | J. Phys. Chem. C 2014, 118, 7307−7320

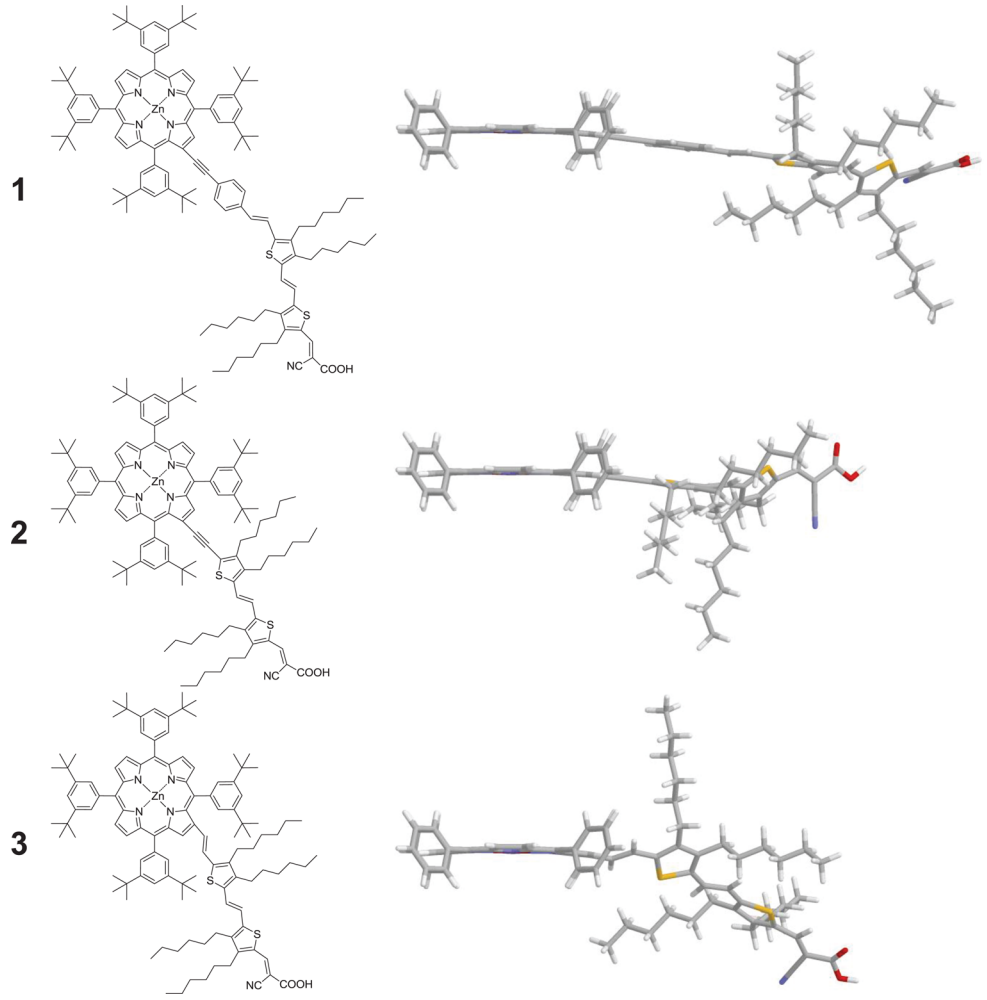


**Figure 1.** Chemical structures (left) and optimized geometries (right) of investigated $Zn^{II}$ porphyrinates.

**Electrochemical Investigation.** The voltammetric studies were performed in a 4 $cm^3$ cell, on 0.0005−0.001 M solutions in dimethylformamide (Aldrich, 99.8%) with 0.1 M tetrabutylammonium perchlorate (TBAP, Fluka) as the supporting electrolyte. In some cases sonication was applied to promote analyte dissolution. The solutions were deaerated by $N_2$ bubbling. The ohmic drop was compensated by the positive feedback technique.[21]

The experiments were carried out using an AUTOLAB PGSTAT potentiostat (EcoChemie, The Netherlands) run by a PC with General-Purpose-Electrochemical-System (GPES) software. Cyclic voltammetry (CV) investigations were carried out at scan rates typically ranging from 0.05 to 2 V $s^{-1}$, with ohmic drop compensation; differential pulse voltammetry (DPV) curves (step potential: 5 mV, modulation amplitude: 50 mV) were also recorded for each compound as both oxidative and reductive scans.

The working electrode was a glassy carbon disk one (AMEL, diameter = 1.5 mm) cleaned by synthetic diamond powder (Aldrich, diameter = 1 $\mu$m) on a wet cloth (STRUERS DP-NAP); the counter electrode was a platinum disk or wire; the operating reference electrode was an aqueous saturated calomel electrode, but the potentials ultimately referred to the $Fc^+/Fc$ couple (the intersolvental redox potential reference currently recommended by IUPAC[22,23]), recording the CV pattern under the same working conditions. To prevent water and chloride leakage into the working solution a compartment filled with the operating medium and fitted with a porous frit was interposed between the reference electrode and the cell.

**Preparation of DSSCs.** DSSCs were prepared adapting a procedure reported in the literature.[24] In order to exclude metal contamination glass or Teflon containers were used. FTO glass plates (7 Ω/sq) were washed in a detergent solution and in EtOH using an ultrasonic bath and rinsed with pure water and absolute EtOH. FTO plates were treated with a freshly prepared 40 mM aqueous solution of $TiCl_4$ for 30 min at 70 °C and then rinsed with water and EtOH. An active monolayer of 10-$\mu$m was screen-printed using a 400-nm nanoparticle opaque paste (Dyesol 18NR-AO); coated films were dried at 125 °C for 6 min and then thermally treated under an air flow at 325 °C for 10 min, 450 °C for 15 min, and 500 °C for 15 min. The heating ramp rate was 5−10 °C/min. The sintered layer was treated again with 40 mM aqueous $TiCl_4$ (70 °C for 30 min), rinsed with EtOH, and heated at 500 °C for 30 min. After cooling to 80 °C the $TiO_2$ coated plate was immersed into a 0.2 mM solution of the porphyrinic dye in EtOH/THF 9:1 containing chenodeoxycholic acid (CDCA, 0.2 mM) for 2 h. In the case of dye N719 the $TiO_2$ coated plate was immersed for 20 h in a 0.5 mM EtOH solution of the dye. The thickness of the layer was measured with a VEECO Dektak 8 Stylus Profiler.


dx.doi.org/10.1021/jp412087f | J. Phys. Chem. C 2014, 118, 7307−7320

**Scheme 1**[a]

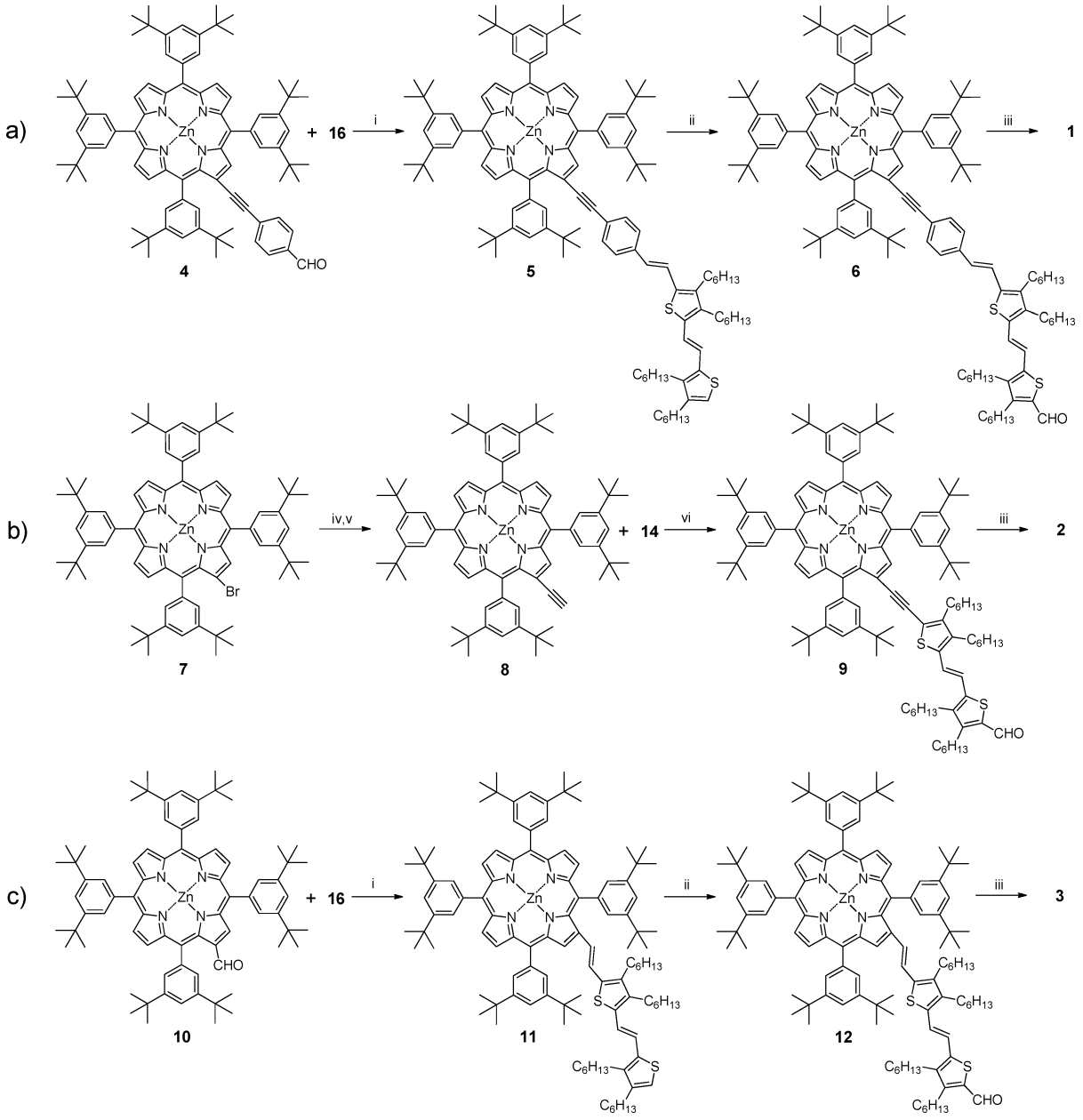


[a]i) t-BuOK, THF, 3 h, r.t.; ii) $POCl_3$/DMF, $CH_2Cl_2$, 18 h, reflux; iii) 2-cyanoacetic acid, piperidine, $CH_3CN/CHCl_3$, 16 h (80 °C); iv) ethynyltrihexylsilane, $Pd(PPh_3)_4$, CuI, $HNEt_2$/DMF (3:1), 1 h, MW (120 °C); v) TBAF, THF, 30 min (25 °C); vi) $PdCl_2(PPh_3)_2$, CuI, $NEt_3$/THF (1:1), 18 h, reflux.

The counter electrode was prepared according to the following procedure. A 1-mm hole was made in a FTO plate using diamond drill bits. The electrode was then cleaned with a detergent solution, 10% HCl, and finally acetone. After heating at 400 °C for 15 min a drop of a $5 \times 10^{-3}$ M solution of $H_2PtCl_6$ in EtOH was added and thermal treatment at 400 °C for 15 min repeated. The dye-coated photoanode and the Pt-counter electrode were assembled into a sealed sandwich-type cell by heating with a hot-melt ionomer-class resin (Surlyn 25-$\mu$m thickness) as a spacer between the electrodes. A drop of the electrolyte solution was added to the hole and introduced inside the cell by vacuum backfilling. Finally, the hole was sealed with a sheet of Bynel.

**Photoelectrochemical Measurements.** Photovoltaic J-V curves were obtained using a 500 W xenon light source (ABET Technologies Sun 2000 class ABA Solar Simulator). The power of the simulated light was calibrated to AM 1.5 (100 mW $cm^{-2}$) using a reference Si cell photodiode equipped with an IR-cutoff filter (KG-5) to reduce the mismatch in the region of 350−750 nm between the simulated light and the AM 1.5 spectrum. J−V curves were obtained by applying an external bias to the cell and measuring the generated photocurrent with a Keithley model 2400 digital source meter. IPCE spectra were recorded as a function of excitation wavelength in AC mode with a chopping frequency of 1 Hz and a bias of white light (0.3 sun). Electrochemical Impedance Spectroscopy (EIS) spectra were obtained using an Eg&G PARSTAT 2263 galvanostat-


dx.doi.org/10.1021/jp412087f | J. Phys. Chem. C 2014, 118, 7307−7320

**Scheme 2**[a]

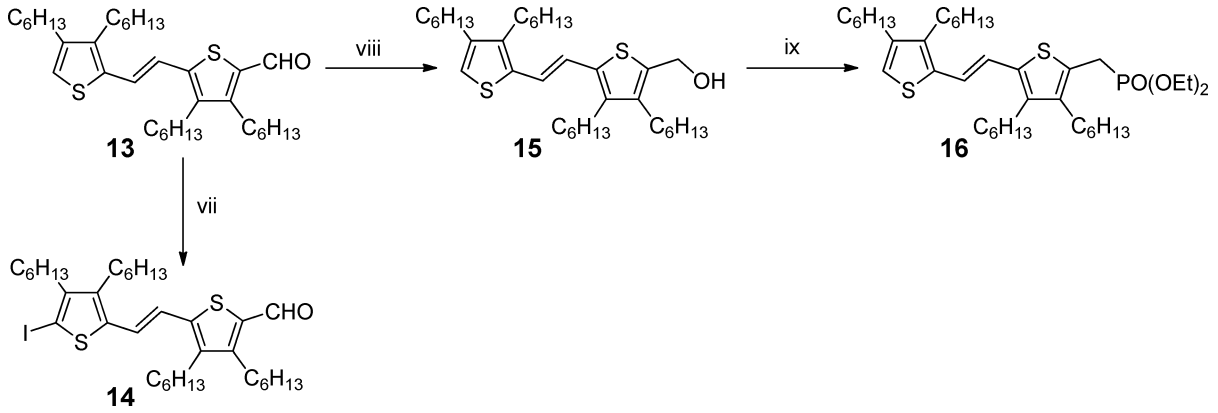


[a]vii) NIS/$CH_3COOH$, $CHCl_3$, 16 h, r.t.; viii) $NaBH_4$, $CH_2Cl_2/CH_3OH$ (1:1), 15 min (0 °C); ix) $PBr_3$/toluene-benzene (2:1), −5 °C, then $HP(OEt)_2$, NaH/THF, 1 h (−20 °C), then 2 h, reflux.

potentiostat. Measurements were performed in the 100 kH 0.1 Hz frequency range using an AC stimulus of 10 mV under 250 W $m^{-2}$ (0.25 sun) illumination under open circuit conditions (no applied bias voltage).

## RESULTS AND DISCUSSION

**Synthesis.** In a recent work Langa, Bisquert et al.[9] have reported the synthesis of a well engineered porphyrinic system consisting of a DTE unit connecting the cyanoacrylic anchoring group and the *meso* position of a triaryl $Zn^{II}$ porphyrinate ring through a styryl bridge. The elongation of the $\pi$ conjugation in this combined system significantly increased absorption intensity and light harvesting in the 450−650 nm region, producing a remarkable improvement of IPCE intensity in this region and, as a consequence, a considerable enhancement of the DSSC performance.

Hence, inspired by this work,[9] we synthesized a series of $Zn^{II}$ porphyrinates **1**, **2**, and **3** (Figure 1) to be investigated as DSSC dyes, with a DTE unit bearing the cyanoacrylic anchoring group connected to the $\beta$ position of a [5,10,15,20-tetrakis(3,5-di-*tert*-butylphenyl) porphyrinate]$Zn^{II}$ ring by a 4-ethynylstyryl system or simpler ethynyl or ethenyl bonds. The aim was to assess the effect of these $\pi$ delocalized substituents on the IPCE spectra and consequently on the DSSC performances of these dyes.

Three different approaches were used to synthesize porphyrinic dyes **1**, **2**, and **3**. Dye **1** was prepared by a Horner-Wadsworth-Emmons reaction between phosphonate thienyl system **16** and porphyrinic aldehyde **4** followed, first by a Vilsmeier formylation of the terminal thienylic unit of **5**, then by a Knoevenagel condensation with cyanoacetic acid of **6** (Scheme 1a). Intermediate **16** was obtained starting from aldehyde **13**[11] as summarized in Scheme 2, while porphyrinic aldehyde **4** was synthesized by an effective Sonogashira coupling based on a microwave-enhanced reaction as recently reported by some of us.[8] The synthesis of **2** with an ethynylic bridge between the DTE unit and the porphyrinic ring (Scheme 1b) was carried out *via* a classical Sonogashira coupling reaction between ethynyl intermediate **8** and iodo derivative **14** (Scheme 2), followed by a Knoevenagel condensation on aldehyde **9**. Attempts to increase yields of the synthesis of this latter precursor by a microwave-assisted Sonogashira reaction failed since significant *E*/*Z* isomerization of the double bond of the DTE unit was repeatedly produced. Although conventional cross-coupling reactions involving the $\beta$-pyrrolic position are generally not very efficient, a good yield (63%) was achieved, without having to apply microwave irradiations, probably due to the high reactivity of the iodo derivative **14**. Conversely intermediate **8** was obtained by using the microwave-enhanced synthetic approach starting from the bromo-porphyirinate **7**, as previously reported.[8]

Dye **3** was synthesized using the same procedure employed for dye **1** (Scheme 1c). A Horner-Wadsworth-Emmons reaction was carried out between phosphonate intermediate **16** and porphyrinic aldehyde **10** obtained as reported in the literature.[13] The formylation of the terminal thienyl unit of **11** followed by the Knoevenagel condensation of **12** with cyanoacetic acid yielded dye **3**.

**Energy Levels and Electron Density Distribution of Molecular Orbitals.** We have carried out a computational DFT and TDDFT investigation on $Zn^{II}$ porphyrinates **1**−**3** in order to compare energy and electron density distribution of their ground and excited state levels (see the Experimental Section). A similar theoretical investigation was recently reported by some of us[8] for a $Zn^{II}$ porphyrinate substituted in the $\beta$ position but with no DTE unit. A preliminary conformation analysis was performed for dye **1**. In particular, several starting structures were studied to assess the planarity/nonplanarity of the DTE bridge and the anchoring group and its influence on the electronic properties. All structures exhibited similar optimized geometry, and the electronic properties did not substantially change. The conformers studied are reported in the SI (Figure 1S).

In the optimized geometry of dyes **1** and **2** the thiophenic moiety of the DTE unit closer to the porphyrinic ring is essentially coplanar with the ring. A sizable deviation from planarity of the thiophenic moiety carrying the cyanoacrylic group is instead found for both **1** (43°) and **2** (59°). In dye **3** both the thiophenic rings of the DTE unit lie out of the porphyrinic plane and are considerably twisted, due to the steric hindrance between the aryl rings in the *meso* position and the thiophenic ring, so that the $\pi$ chain linked to the $\beta$ position of the porphyrin ring assumes a boat-like shape (Figure 1).

The energies of molecular HOMO and LUMO orbitals, computed in THF solution on the optimized geometries of **1**−**3**, are reported in Table 2 and Figure 2, which gives a schematic energy diagram with particular emphasis on the HOMO−LUMO gap. The isodensity plots for **1**−**3** of the electron


dx.doi.org/10.1021/jp412087f | J. Phys. Chem. C 2014, 118, 7307−7320

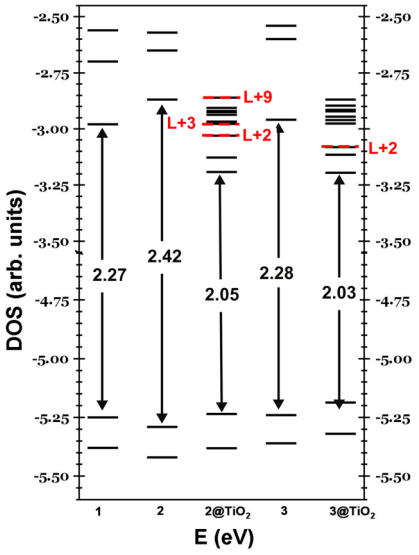


**Figure 2.** Energy level scheme of the main occupied and unoccupied MO and HOMO−LUMO (eV) gap computed in THF on the optimized structures.

density distribution of the molecular orbitals from HOMO-3 to LUMO+3 are reported in Figure 3.

HOMO and LUMO energy levels and consequently HOMO−LUMO energy gap of **1** and **3** are very similar. Some differences are observed with respect to **2**, which exhibits a slightly more stable HOMO energy level but with a LUMO about 0.10 eV above that of **1** and **3**. This leads to an increase in the HOMO−LUMO gap of **2** (2.42 eV) compared to **1** and **3** (2.27 and 2.28 eV, respectively) (Figure 2).

From Figure 2 it appears that the way of linking the $\pi$-delocalized DTE unit to the porphyrinic core may have some relevance.

The key assumption underpinning the four orbital Gouterman model[25] of the electronic structure of the metal porphyrinic core is that in $Zn^{II}$ tetraaryl porphyrinates the HOMO and HOMO-1 levels are near degenerate and the LUMO and LUMO + 1 levels are degenerate.

In our previous investigation[8] we showed that a simple substituent carrying the cyanoacrylic group in the $\beta$ position significantly affects the degeneracy of the two LUMOs. It was shown that the energy difference between LUMO and LUMO + 1 was more than 0.6 eV, while the relative energy of the HOMO and HOMO-1 levels was not influenced as much.

Figure 2 confirms that the presence of a $\pi$ delocalized substituent in the $\beta$ position as in **1**−**3** produces a significant

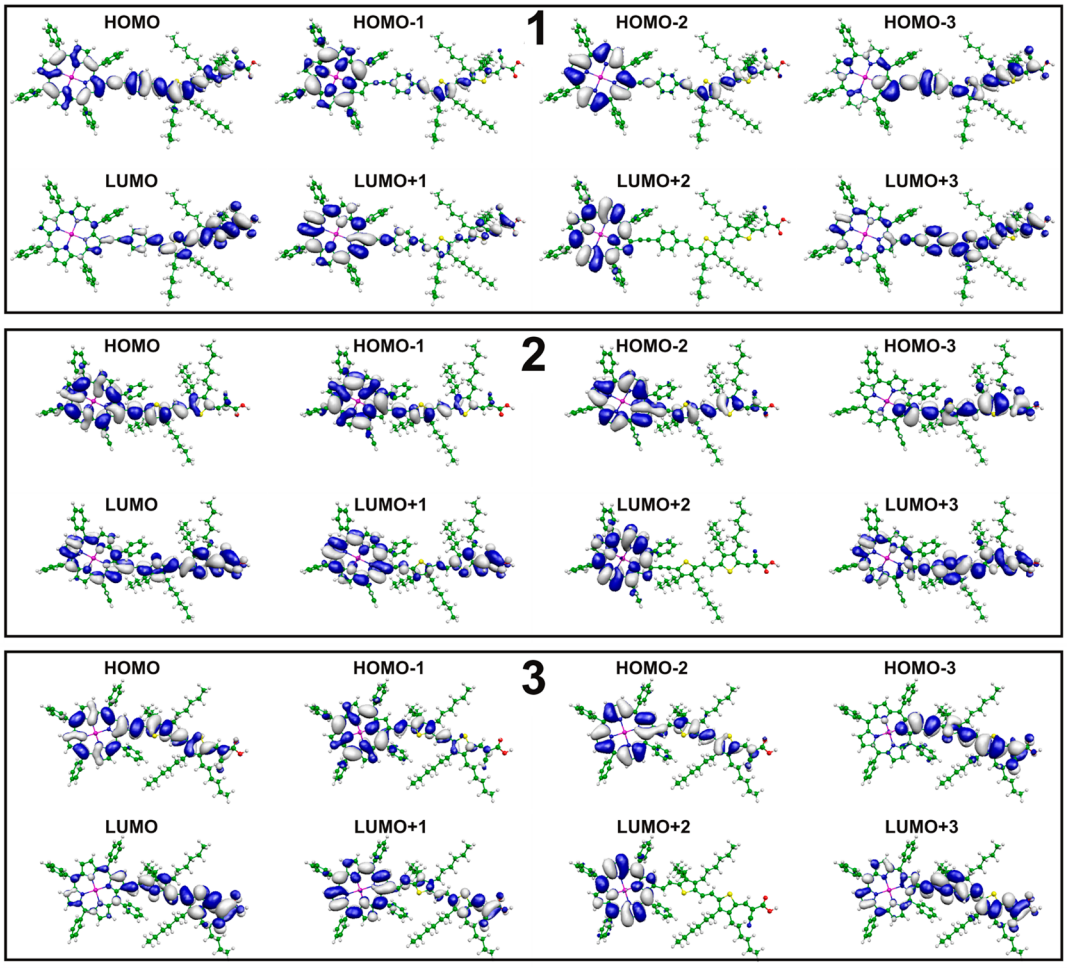


**Figure 3.** Isodensity plots (cutoff = 0.03) computed in THF solution by a DFT approach, of the electron density distribution of the first occupied/unoccupied molecular orbitals of dyes **1**−**3**.


dx.doi.org/10.1021/jp412087f | J. Phys. Chem. C 2014, 118, 7307−7320

effect on the degeneracy of the first two LUMOs, while only a minor effect is observed on the degeneracy of the two HOMOs.

In particular the LUMO orbital of dye **3**, with an ethenylic bridge, shows a significant electronic density on the $\pi$ bridge and on the DTE unit carrying the cyanoacrylic group but an irrelevant electronic density on the porphyrinic core. Conversely the LUMO + 1 orbital is characterized by a relevant electronic density on the cyanoacrylic group but by a lower electron density on the $\pi$ bridge and on the DTE unit and a significant electronic density on the porphyrinic core. On the contrary in dye **2**, with an (*E*) ethynylic bridge, a more significant electronic density is observed on the porphyrinic core both in the LUMO and particularly in the LUMO+1 orbitals (Figure 3).

It follows that the LUMO and the LUMO+1 of dye **2** are characterized by an electron density delocalized over the entire molecule. For dye **3** the charge is mainly localized on the DTE and anchoring group (LUMO) and delocalized over the entire molecule (LUMO+1) resulting in a greater energy difference between the two orbitals compared to dye **2** (see Figure 2).

Moreover **2** and **3** appear to have a similar HOMO electron density distribution, although that of dye **3** exhibits a slightly higher localization on the $\pi$ chain and in particular on the anchoring cyanoacrylic group (Figure 3). This picture results in a stabilization of the LUMO and in a smaller HOMO−LUMO energy gap for dye **3** with respect to dye **2** (Figure 2).

Surprisingly, the introduction of a styryl system bridging the DTE as in dye **1** seems to have no significant impact on the energy or the electron density distribution of either the first occupied HOMO or unoccupied LUMO molecular orbitals, if compared to that observed for dye **3**. Therefore the HOMO−LUMO energy gap is quite comparable (Figures 2 and 3). Interestingly, the HOMO and HOMO-1 orbitals of **1** and **3** show different localizations of electron density (more localized on the porphyrin + bridge and porphyrin, respectively), while those of dye **2** show similar localization (more centered on the porphyrin + bridge) (Figure 3).

In order to produce a large electronic transfer toward the cyanoacrylic anchoring group by excitation in dyes **1**−**3**, the transition must involve higher excited levels, such as that which occurs in the HOMO → LUMO+3 transition. In fact the LUMO+3 orbital is characterized, in all dyes **1**−**3**, by a high electron density localized on the $\pi$ delocalized $\beta$ substituent and in particular on the cyanoacrylic group with a limited electronic density on the porphyrinic core (Figure 3).

Finally, in order to investigate the origin of the different photovoltaic performance of the dyes in DSSC, we calculated the electronic structure of 2@$TiO_2$ and 3@$TiO_2$ clusters formed by dyes **2** and **3** adsorbed onto a model of 82 $TiO_2$ units of the semiconductor surface, as previously reported by some of us for a similar cluster based on dye **1** of ref 8.

For each considered system, the contribution of the dye LUMO to the unoccupied electronic states of the interacting dye-semiconductor system was evaluated by calculating the percentage weight of the dye orbital on the total Density of States (DOS). In other words, we evaluated the dye partial DOS (PDOS) reconstructing the dye LUMO contribution among the 100 lowest unoccupied states of the interacting dye-semiconductor system. The broadening of such PDOS, plotted by a Gaussian convolution in Figures 4 and 5, can be related in the Newns-Aderson framework[26] to the inverse of the injection time from the dye LUMO to the semiconductor manifold of unoccupied states.

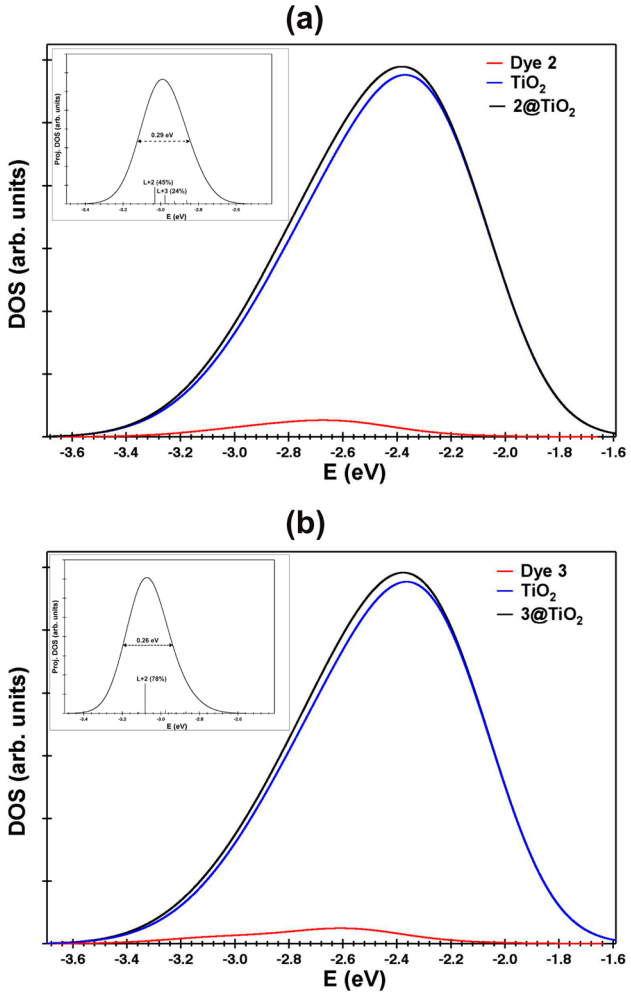


**Figure 4.** Density of unoccupied states of the cluster dye@$TiO_2$. Total cluster: black line, $TiO_2$: blue line, Dye: red line. The inset shows the projection of the LUMO of the dye on the cluster dye@$TiO_2$ together with the full width at maximum height (FWMH) for dye **2** (a) and **3** (b).

The results show that the broadening of the dye LUMO in the presence of the semiconductor is slightly higher for dye **2** than for dye **3**. Indeed, the fwhm (full width at half-maximum) of the LUMO PDOS is 0.29 and 0.26 eV for 2@$TiO_2$ and 3@$TiO_2$, respectively.

Although this difference is quite small, it is suggestive evidence of the different interaction accompanying dye **2** and **3** adsorption onto $TiO_2$. In fact, when the link occurs through an ethynylic bridge, as in dye **2**, we find several orbitals with relevant dye contributions. In particular we have calculated various states with a dye contribution higher than 10% (LUMO +2 at −3.03 eV with 45%, LUMO+3 at −2.98 eV with 24%, and LUMO+9 at −2.86 eV with 11%) plus the LUMO+6 at −2.93 eV with 9% dye contribution (Figure 4a). On the contrary for dye **3** mixing and broadening is much lower, and the LUMO of the dye is mainly concentrated in the LUMO+2 state of the 3@$TiO_2$ system, with a dye contribution of 78%. LUMO+3 is mainly localized on the semiconductor with a minor electron density on the DTE unit and the anchoring cyanoacrylic group of 8% (Figure 4b). For both dyes the LUMO and the LUMO +1 are almost completely located on the semiconductor.


dx.doi.org/10.1021/jp412087f | J. Phys. Chem. C 2014, 118, 7307−7320

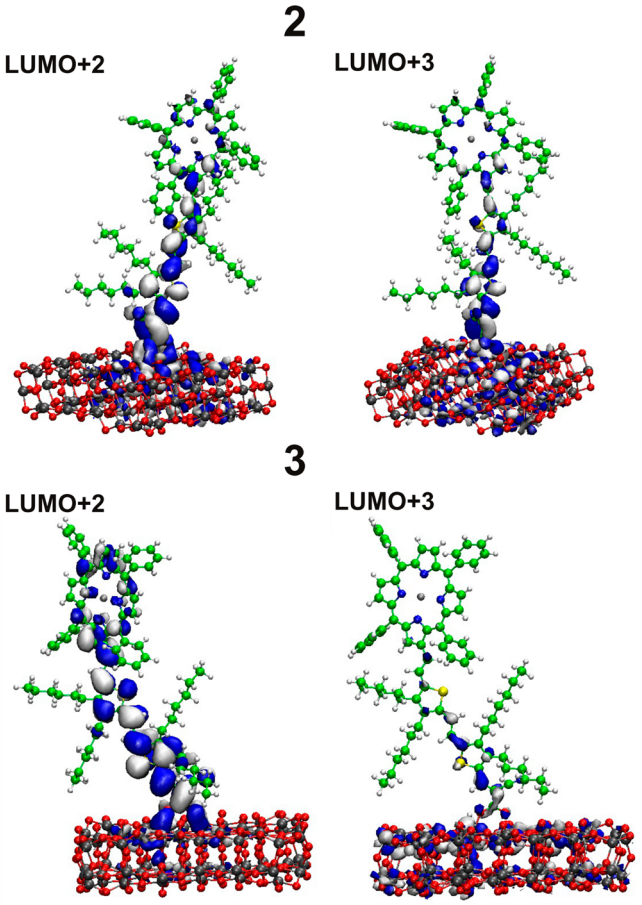


**Figure 5.** Electron density distribution of the LUMO+2 and LUMO+3 molecular orbitals of the 2@$TiO_2$ (top) and 3@$TiO_2$ (bottom) cluster where the LUMOs of the dye **2** and **3** are mainly located.

**Experimental and Computed Electronic Absorption Spectra and Experimental Emission Spectra.** Electronic absorption spectra in THF solution of $Zn^{II}$ porphyrinates **1**−**3** are reported in Figure 2S. The corresponding absorption data, both experimental and computed by TDDFT calculations, are summarized in Table 1. To check the validity of the functional used absorption spectra have also been generated using CAM-B3LYP. The results, reported in the SI together with the experimental data and the B3LYP computed transitions, evidence that B3LYP shows better agreement over the entire investigated spectral range (Table 1S).

In addition to typical B and Q bands, $Zn^{II}$ porphyrinates **1**−**3** show a broad and relatively intense absorption band between 490 and 530 nm, more intense for **2.** This absorption is originated by the $\pi$ delocalized substituent in the $\beta$ position, containing a DTE unit. The B bands of dyes **1**−**3** show comparable intensity, and the Q-band at lower energy is slightly red-shifted going from **1** to **3** (Table 1). In the range of wavelengths typical of the B absorption band, only one electronic transition was calculated for dyes **1**−**3**; moreover when we consider the composition in terms of transitions that give rise to the B band, TDDFT calculations support a relevant contribution, particularly for **1**, of the HOMO → LUMO+3 transition (Table 1). As pointed out above, the HOMO→ LUMO+3 transition is characterized by a relevant electron transfer from the porphyrinic core to the $\pi$ delocalized substituent in the $\beta$ position and specifically to the cyanoacrylic group, thus producing a significant charge separation.

HOMO-2 → LUMO+1 transition also contributes to the B band of **1**−**3**, mainly localized on the porphyrinic core, with a limited electron transfer to the $\pi$ delocalized substituent in the $\beta$ position. The HOMO-1 → LUMO+2 transition, with a limited contribution to the B band of **2** and **3**, is also mainly localized on the porphyrinic core (Table 1 and Figure 3).

In summary a charge transfer process from the porphyrinic core to the $\pi$ delocalized substituent in the $\beta$ position partially

**Table 1. Experimental and Computed Electronic Absorption Spectra and Experimental Emission Spectra in THF Solution of the $Zn^{II}$-Porphyrinates 1−3**

| | absorption | | | | | | emission |
|---|---|---|---|---|---|---|---|
| dye | B bands $\lambda_a$ (nm) [log $\varepsilon$] | comp. B bands[a] $\lambda_a$ (nm) [Int. (au)] | sharp bands $\lambda_a$ (nm) [log $\varepsilon$] | comp. Sh. bands[a] $\lambda_a$ (nm) [Ing (au)] | Q bands $\lambda_a$ (nm) [log $\varepsilon$] | comp. Q bands[a] $\lambda_a$ (nm) [Int. (au)] | Em. $\lambda_e$ (nm) |
| **1** | 436 [5.27] | 447 [1.21] (77% H→L+3) (17% H-2→L+1) | 493 [4.74] | 498 [0.15] (72% H-2→L) 524 [0.21] (38% H→L+2) (27% H-1→L+1) (15% H-2→L) | 566 [4.67] 603 [4.36] | 545 [0.14] (48% H-1→L) (14% H→L+1) (12% H→L+2) 630 [2.51] (90% H→L) | 626 668 |
| **2** | 434 [5.30] | 425 [1.26] (35% H→L+3) (34% H-2→L+1) (12% H-1→L+2) | 511 [4.92] | 520 [0.23] (31% H-1→L) (28% H→L+1) (20% H→L+2) | 571 [4.66] 609 [4.67] | 549 [0.33] (40% H→L+1) (24% H-1→L+2) 600 [1.34] (80% H→L) | 635 673 |
| **3** | 432 [5.24] | 424 [1.22] (33% H→L+3) (30% H-2→L+1) (12% H-1→L+2) | 527 [4.75] | 521 [0.10] (33% H-2→L) (27% H-1→L+1) (27% H→L+1) | 566 [4.62] 612 [4.55] | 556 [0.22] (31% H-1→L+2) (26% H→L+1) (12% H→L+2) 630 [1.72] (87% H-1→L) | 631 674 (sh) |

[a]The nature and composition of the transitions involved in each computed absorption band is reported in parentheses.


dx.doi.org/10.1021/jp412087f | J. Phys. Chem. C 2014, 118, 7307−7320

Table 2. Key CV Features of the $Zn^{II}$ Porphyrinates 1−3 and Electrochemical Energy Levels HOMO and LUMO Derived Therefrom[d]

| [a] | $\lvert E_{p,Ic} - E_{p,IIc}\rvert$/V ($Fc^+$\|Fc) | $E^\circ_{Ic}$/V($Fc^+$\|Fc) | $E^\circ_{Ia}$/V($Fc^+$\|Fc) | $\lvert E_{p,IIa} - E_{p,Ia}\rvert$/V($Fc^+$\|Fc) | LUMO/eV[b] | HOMO/eV[b] | $E_g$/eV[b] | LUMO (Th.)/eV[c] | HOMO (Th.)/eV[c] | $E_g$ (Th.)/eV[c] |
|---|---|---|---|---|---|---|---|---|---|---|
| **1** | 0.42 | **−1.70** | **0.36** | 0.15 | **−3.10** | **−5.16** | **2.06** | −2.98 | −5.25 | 2.27 |
| **2** | 0.42 | **−1.70** | **0.39** | 0.25 | **−3.10** | **−5.19** | **2.09** | −2.87 | −5.29 | 2.42 |
| **3** | 0.43 | **−1.70** | **0.33** | 0.17 | **−3.10** | **−5.13** | **2.02** | −2.96 | −5.24 | 2.28 |
| **ZnTdTbPP** | 0.45 | **−1.84** | **0.36** | 0.32 | **−2.96** | **−5.20** | **2.20** | | | |
| **DTE** | | **−2.53** | **0.56** | | **−2.27** | **−5.36** | **3.09** | | | |

[a]ZnTdTbPP = $Zn^{II}$(tetraditerbutylphenylporphyrinate); DTE = (*E*)dithienylethylene. [b]Electrochemical values, $E_g$ is the HOMO−LUMO energy gap. [c]DFT computed values in THF solution, $E_g$ is the HOMO−LUMO energy gap. [d]$E^\circ_{Ic}$ and $E^\circ_{Ia}$ (or $E_{p,Ic}$ and $E_{p,Ia}$), all referring to the ferrocene couple, are also reported for ZnTdTbPP and for dithienylethylene[31] (obtained in MeCN but referring to the ferrocene couple). For the sake of comparison the computed HOMO and LUMO in THF solution of **1**−**3** are also reported.

contributes to the B band, particularly in the case of dye **1**, thus confirming a not trivial role of the B band in the generation of charge separation by light absorption, as previously suggested by some of us.[8]

Moreover TDDFT calculations show that the main transition contributing to the Q-band at lower energy of dyes **1** and **2** is the HOMO→LUMO transition. This involves a significant electron density transfer from the porphyrinic core to the $\pi$ delocalized substituent in the $\beta$ position and particularly to the anchoring cyanoacrylic group (Table 1 and Figure 3). Interestingly for dye **3** the main transition contributing to the Q-band at lower energy is the HOMO-1→ LUMO transition which still involves a similar electron transfer process (Figure 3).

Major contributions to the Q-band at higher energy are given by HOMO-1 → LUMO, HOMO → LUMO+1, and HOMO-1 → LUMO+2 transitions, mainly localized on the porphyrinic core. The exception is HOMO-1→LUMO transition (Table 1), which involves some electron transfer from the porphyrinic core to the $\beta$ substituent (Figure 3), and is significant only for dye **1**. A limited contribution, for dyes **1** and **3**, is given by the HOMO→ LUMO+2 transition, which involves some opposite electron transfer from the $\pi$ delocalized $\beta$ substituent to the porphyrinic core (Table 1 and Figure 3).

For the electronic absorption bands in the range 490−530 nm, TDDFT calculations support different contributions for **1**, **2**, and **3**. In particular the transitions HOMO-2 →LUMO and HOMO→LUMO+2 are predominant for **1**; HOMO-1→ LUMO and HOMO→LUMO+1 are predominant for **2**; and HOMO-2→LUMO and HOMO → LUMO+1 are predominant for **3** (Table 1). Since these transitions and, in particular, the HOMO-2→LUMO involve the porphyrinic core (Figure 3), it follows that these absorptions are not to be attributed only to $\pi$−$\pi^*$ transitions localized on the $\pi$ chain of the substituent, since some electron transfer from the porphyrinic core to the substituent in the $\beta$ position (HOMO-2→LUMO) and vice versa (HOMO→LUMO+2) is involved (Figure 3). This evidence confirms some $\pi$ conjugation along the entire molecular structure of **1**−**3**, thus producing a perturbation of the Gouterman four orbital model.[25]

**Electrochemical Investigation.** The electronic properties of $Zn^{II}$ porphyrinates **1**−**3** have been investigated by cyclic voltammetry. CV patterns obtained at 0.2 V $s^{-1}$ on the GC electrode in DMF + 0.1 M TBAP are reported in Figure 3S, and their key features are summarized in Table 2.

In all cases more than one oxidation and reduction peak is observed in the potential window investigated. The first is reversible or quasi reversible from both the electrochemical and chemical point of view, affording calculation of formal potentials of the first oxidation (anodic) $E^{\circ\prime}_{S|S+}$ and the first reduction (cathodic) $E^{\circ\prime}_{S-|S}$ process of the dye S in the operating solvent (formal potentials $E^{\circ\prime}$ approximate standard potentials $E^\circ$ under the assumption of neglecting activity coefficients)

$$E^{\circ\prime}_{S|S+} = (E_{rev\,Ia,forward} + E_{rev\,Ia,backward})/2 \approx E^\circ_{S|S+} \quad (1a)$$

$$E^{\circ\prime}_{S-|S} = (E_{rev\,Ic,forward} + E_{rev\,Ic,backward})/2 \approx E^\circ_{S-|S} \quad (1b)$$

The corresponding absolute standard energies for the first oxidation and the first reduction process of dye S, $\Delta G^\circ_{S|S+}$ and $\Delta G^\circ_{S-|S}$ respectively, were thus evaluated according to the following relationships:[27]

$$\Delta G^\circ_{S|S+}(eV) = -e \times [(E^\circ_{S|S+}/V(Fc^+|Fc) + 4.8\ V(Fc^+|Fc\ vs\ zero)] \quad (2)$$

$$\Delta G^\circ_{S-|S}(eV) = -e \times [(E^\circ_{S-|S}/V(Fc^+|Fc) + 4.8\ V(Fc^+|Fc\ vs\ zero)] \quad (3)$$

These absolute standard energies are commonly termed electrochemical HOMO and LUMO energy levels and allow evaluation of the electrochemical energy gaps $E_g$ (Table 2).

As previously reported[8,28] for structurally related $Zn^{II}$ porphyrinates with an asymmetric structure, the $E^\circ_{Ia} - E^\circ_{Ic}$ values (Table 2) are significantly smaller than the lower boundary of the well-known Kadish relationship[29,30] holding for symmetrical structures such as tetraphenylporphyrin (TPP) and diphenylporphyrin (DPP) templates

$$E^\circ_{Ia} - E^\circ_{Ic} = 2.25 \pm 0.15\ V \quad (4)$$

which instead fully holds for the symmetrical $Zn^{II}$ tetraditerbutylphenylporphyrinate (ZnTdTbPP) (Table 2). This observation is consistent with both an effect due to the electronic conjugation between the porphyrinic core and the thiophenic $\pi$ delocalized substituent in the $\beta$ position and/or the localization of one or both of the first oxidation and reduction processes in a more favorable site than the porphyrinic core.

The first oxidation potentials of **1**−**3** (0.36, 0.39, 0.33 V respectively), almost coincide with that of ZnTdTbPP (0.36 V ($Fc^+$|Fc)). However, the electron rich (*E*)-DTE unit of the substituent in the $\beta$ position could also become a favorable oxidation site, due to its intrinsic oxidation potential. Although more positive than that of ZnTdTbPP ($E^\circ_{Ia}$ DTE = 0.56 V ($Fc^+$|Fc),[31] Table 2), its potential could be significantly decreased by two factors. The first are inductive effects since


dx.doi.org/10.1021/jp412087f | J. Phys. Chem. C 2014, 118, 7307−7320

each of the four alkyl substituents of the thienyl group can contribute with a positive shift of about 0.05 V, i.e. about 0.2 V globally, according to the reference case of alkylferrocenes in the same solvent.[32] The second is the possible role of the bridging double and/or triple bond of the $\pi$ chain containing the DTE unit, in increasing effective conjugation and therefore affording better stabilization of the radical cation located on the DTE unit. It follows that, although the antagonist electron withdrawing inductive effect by the cyanoacrylic anchoring group should also be taken into account, it is possible that the above two effects prevail, making the DTE unit comparable or even competitive with the porphyrinic core as first oxidation center.

A further hint comes from the distance between the first and second oxidation peak. In fact, two redox sites of comparable energy (e.g., in the case of "equivalent redox centers") result in two subsequent CV peaks, whose $E_{p,IIa} - E_{p,Ia}$ difference accounts for the reciprocal repulsive interaction between the two charged centers.[33] Accordingly, the $E_{p,IIa} - E_{p,Ia}$ difference decreases (i) by decreasing the conjugation efficiency at constant distance between the two redox centers (e.g., substituting a saturated system connecting the two redox sites with an unsaturated one)[34] and/or (ii) with the same conjugation efficiency, by increasing the distance between the two redox sites.[34] Accordingly, in the linear $\alpha$-oligothiophene $T_n$ series of high conjugation efficiency, the $E_{p,IIa} - E_{p,Ia}$ difference, which accounts for charge repulsion in the dication species, decreases from 0.95 V for $T_3$ to 0.44 V for $T_4$ and 0.27 V for $T_6$.[34]

In the case of ZnTdTbPP, both the first and second oxidation processes are centered on the porphyrinic core, and the reciprocal interaction between the two positive charges on the porphyrinic ring corresponds to a 0.32 V $E_{p,IIa} - E_{p,Ia}$ difference between the first two oxidation potentials (Table 2). However, this difference is remarkably lower in dyes **1** and **3** ($E^\circ_{IIa} - E^\circ_{Ia}$ = 0.15 V and 0.17 V, respectively, Table 2 and Figure 3S), with the DTE unit linked to the $Zn^{II}$ porphyrinate ring or to the 4-phenylethynyl $Zn^{II}$ porphyrinate system by a (*E*)-ethenyl bridge, resulting in two quite close oxidation peaks. Although, differently from case **2**, the second oxidation peak can be neatly observed only at scan rates higher than ∼0.1 V/s (with concurrent increase in the first oxidation peak reversibility) (Figure 4S), suggesting a mechanism more complex than that of case **2** and worthy of specific mechanistic investigation, the closeness of the two oxidation peaks in **1** and **3** could point to two redox sites of comparable energy and very low reciprocal interaction. Actually, considering the isodensity plots of **1** and **3** (Figure 3), a significant difference is perceivable in the electron density localization of the HOMO and HOMO-1 orbitals, respectively. In both cases the electron density on the HOMO is mainly centered on the $\pi$ chain containing the DTE unit and that of the HOMO-1 on the porphyrinic ring, respectively. This evidence would support the assumption that in **1** and **3** the first and second oxidation processes are centered on two significantly separated sites (the porphyrinic ring and the DTE unit, respectively) and can therefore take place at closer energies. Similarly, some of us have reported asymmetric porphirinic systems with a substituent carrying an amino terminal, where the first two oxidations, localized on the amino terminal and porphirinic ring, respectively, take place at very close potentials.[28] This suggests a significant involvement of the double bond in bridging the DTE unit to the porphyrinic system, making DTE a competitive oxidation center with the porphyrinic core. Even assuming some $\pi$ conjugation between the two oxidation centers, their significant distance would generate a small $E^\circ_{IIa} - E^\circ_{Ia}$ difference (as in the polythiophene case mentioned above).

Remarkably, when the linking bridge is an ethynyl bond as in **2**, the distance between oxidation peaks is greater ($E^\circ_{IIa} - E^\circ_{Ia}$ = 0.25 V), midway between that of **1**, **3**, and ZnTdTbPP. This evidence, again, appears fully consistent with the isodensity plots (Figure 3), which show that in **2**, HOMO and HOMO-1 orbitals nearly coincide and are mainly localized on the porphyrinic core, only partially extending toward the conjugated $\pi$ system, containing the DTE unit, through the bridging triple bond. This implies that the two positive charges can be positioned slightly farther away than in ZnTdTbPP but not as far away as in **1** and **3**.

In conclusion, the double or triple bond nature of the bridge seems to act as a sort of switch between the two different situations.

Also the localization of the first reduction site is not straightforward. The electron withdrawing cyanoacrylic group linked to the DTE unit could provide a favorable reduction site, since its reduction potential is not far from the value $E^\circ_{Ic} \approx -1.9$ V($Fc^+$|Fc), reported for that of a cyanoacrylic group linked to a linear benzodithiophene system conjugated to a further ethylene group.[35] However, since the first reduction site of ZnTdTbPP is at $E^\circ_{Ic} = -1.84$ V (Table 2) also the porphyrinic core may be competitive as the first reduction site.

However, quite unlike the oxidation process, the CV reduction peaks coincide in shape, position, and $E^\circ_{Ic} - E^\circ_{IIc}$ difference for all dyes **1**−**3**, pointing to a similar process taking place. In fact, the first reduction potential (−1.7 V), the same for **1**−**3**, is significantly less negative than that of ZnTdTbPP (−1.84 V ($Fc^+$|Fc)) and than that reported above for a cyanoacrylic group linked to a $\pi$ conjugated system (∼−1.9 V ($Fc^+$|Fc)[35]). Since the difference $E^\circ_{Ic} - E^\circ_{IIc}$ between the first and second reduction potentials of **1**−**3** is only slightly lower than that of ZnTdTbPP, this also points to a significant interaction between the two negative charges.

Finally as for the electrochemical HOMO and LUMO energy levels and $E_g$ gaps (Table 2), they are quite similar for **1**−**3**, and they fully comply with the requirement of a DSSC cell.[30]

It must be underlined that the electrochemical and DFT computed HOMO and LUMO energy levels of **1**−**3** show consistent trends but do not have to coincide (Table 2).

Therefore in order to investigate the accuracy of our DFT theoretical calculations we used a theoretical methodology developed by some of us[19,36] to calculate the so-called excited state oxidation potentials (ESOP) and ground state potential (GSOP), in dye **3** in THF solution.

Using this approach we yielded for **3** a GSOP value of 5.05 eV and an ESOP value of 3.08 eV to be compared with the experimental electrochemical $\Delta G^\circ_{S|S+}$ value of 5.13 eV and $\Delta G^\circ_{S-|S}$ value of 3.10 eV. The excellent agreement achieved confirms the accuracy of our theoretical approach. Indeed GSOP and ESOP parameters provide a more appropriate comparison with electrochemical parameters, either as electrochemical HOMO and LUMO levels or as $\Delta G^\circ_{S|S+}$ and $\Delta G^\circ_{S-|S}$, since they afford to take into account molecular charged states and the significant effects due to the strong solvation energy.

**Photoelectrochemical Investigation.** $Zn^{II}$ porphyrinates **1**−**3** have been applied as dyes in DSSCs, prepared using an opaque active $TiO_2$ layer of 10 $\mu$m as photoanode. The photoanode was immersed for 2 h in a EtOH/THF 9:1


dx.doi.org/10.1021/jp412087f | J. Phys. Chem. C 2014, 118, 7307−7320

solution of the dye. Longer immersing times repeatedly afforded lower photovoltaic efficiencies, probably due to a detrimental slow aggregation of the porphyrinic dye on the $TiO_2$ surface. Different electrolytes were tested; the best reproducible photovoltaic efficiencies were obtained with the electrolyte VT8 (0.6 M 1-allyl-3-methylimidazolium iodide, 0.02 M $I_2$, 0.1 m LiI, 0.05 M 4-*tert*-butylpyridine in 3-methoxypropionitrile). We have also investigated the effect of the addition of an equimolar amount, with respect to the porphyrinic dye, of chenodeoxycholic acid (CDCA) as a deaggregating coadsorbent agent but without producing a significant increase of the efficiency. The best photovoltaic parameters and performances of each dye are reported in Table 3, in comparison to those of the benchmark dye N719,

**Table 3. Photovoltaic Characteristics of DSSCs Based on 1−3 as Dyes**

| dye | $J_{sc}$ (mA cm$^{-2}$) | $V_{oc}$ (mV) | FF | PCE [%] |
|---|---|---|---|---|
| **1** | 12.4 | 648 | 0.65 | 5.2 |
| **2** | 11.7 | 658 | 0.61 | 4.7 |
| **3** | 10.5 | 635 | 0.64 | 4.3 |
| N719[a] | 15.9 | 757 | 0.65 | 7.8 |

[a]Electrolyte: 0.6 M *N*-butyl-*N*-methylimidazoliumiodide, 0.03 M $I_2$, 0.10 M guanidinium thiocyanate, and 0.5 M 4-*tert*-butylpyridine in acetonitrile/valeronitrile 85:15.

measured working with the standard electrolyte A6141 under the same experimental conditions. The overall power conversion efficiencies (PCE) were obtained from the equation

$$\mathrm{PCE} = J_{sc} \times V_{oc} \times \mathrm{FF} \quad (5)$$

where $J_{sc}$ is the short circuit current density, $V_{oc}$ is the open circuit voltage, and FF is the fill factor. Figure 6 shows the photocurrent−voltage curves of DSSCs based on dyes **1**−**3**, while the incident monochromatic photon-to-current conversion efficiencies (IPCEs) are depicted in Figure 7.

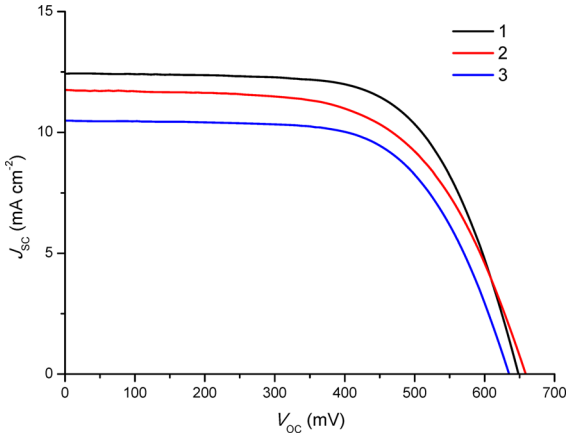


**Figure 6.** Photocurrent−voltage plots of DSSCs based on **1**−**3** as dyes.

In agreement with the findings of Bisquert, Langa et al.[9] the large gain in the electronic absorption spectrum of dyes **1**−**3** in the region 490−530 nm is reflected in their IPCE spectra, characterized by a broad plateau of constant intensity (about 60% for **1** and **2** and 40% for **3**) in the region 430−650 nm with onsets at decreasing energy from **2**, **1**, to **3**.

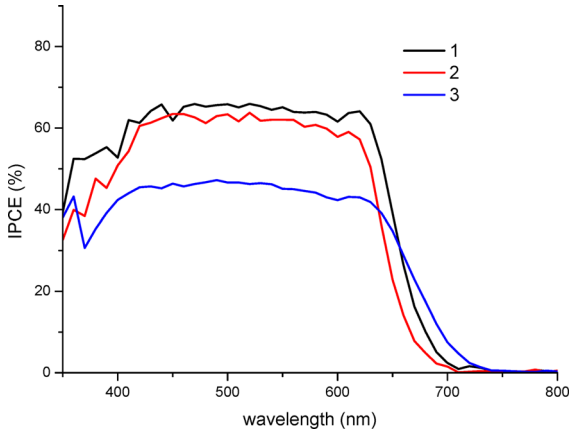


**Figure 7.** IPCE spectra of DSSCs based on **1**−**3** as dyes.

Dyes **1** and **2** produce a similar photocurrent and open circuit voltage, while dye **3** shows a sizably reduced photocurrent (Figure 6 and Table 3). Accordingly, when comparing the IPCE spectra of **1** and **2** versus that of **3**, a significant lower intensity of the plateau is observed. Moreover it appears that the relatively small red-shifted IPCE onset of **3** (Figure 7), which reflects the features of the electronic absorption spectra, (Figure 2S), is not translated into a significant enhancement of its photocurrent.

The much lower intensity of the IPCE plateau and consequently of the photocurrent values of dye **3** compared to the structurally similar dye **2** (Figure 7 and Table 3) are worthy of analysis since the only structural difference between **2** and **3** is the nature of the bridge (ethynylic for **2** and (*E*) ethenylic for **3**) between the porphyrinic core and the thiophenic DTE unit carrying the anchoring cyanoacrylic group (Figure 1).

The most significant electronic difference between **2** and **3** is the slightly larger HOMO − LUMO energy gap of **2** (Figure 2 and Table 2). Dye **2** also differs in terms of the various transitions involved, by configuration interactions, in the broad and intense absorption band in the region 490−530 nm, which is stronger in the case of **2** (Figure 2S and Table 1).

This absorption band is originated not only by $\pi \rightarrow \pi^*$ transitions typical of the $\pi$ chain of the substituent in the $\beta$ position but also by transitions involving some charge transfer processes between the porphyrinic core and the $\pi$ chain. In particular these transitions are quite different when comparing dyes **2** and **3**, since the only one in common is the HOMO→LUMO+1 transition (Table 1).

It follows that the significant difference of the IPCE spectra and of the photocurrent values could be originated by a lower injection efficiency of **3**, when compared to **2.** In fact both **2** and **3** are characterized, with some small differences in the region 490−530 nm, by very similar absorption spectra (Figure 2S and Table 3) thus allowing us to safely assume an efficiency of light harvesting (LHE) close to unit for both dyes.

The increased deviation of the molecular structure of **3** compared to **2**, from the planarity between the porphyrinic ring and the $\pi$ chain of the substituent (in particular the DTE unit) (Figure 1), suggests that **3** has a lower interaction between the porphyrinic core and the $\pi$ chain. This is also supported by the electrochemical investigation which confirms a lower interaction in the case of **3** with respect to **2**.

The effect due to structural differences between **2** and **3** seems to be confirmed by the DFT calculations on the nature


dx.doi.org/10.1021/jp412087f | J. Phys. Chem. C 2014, 118, 7307−7320

of the electronic interaction of dyes **2** and **3** with a model of the $TiO_2$ surface made by a cluster of 82 $TiO_2$ units. This supports a slightly lower injection efficiency of **3** when compared to **2** (Figures 4 and 5).

Finally in order to exclude a possible difference of the electronic effects produced by **2** and **3** on the charge recombination process between electrons localized in the conduction band of the $TiO_2$ semiconductor and $I_3^-$ ions of the electrolyte, and consequently on the photocurrent, an electrochemical impedance spectroscopy (EIS) investigation was carried out. The analysis of the impedance spectra was performed in terms of Nyquist plots (Figure 8) where the

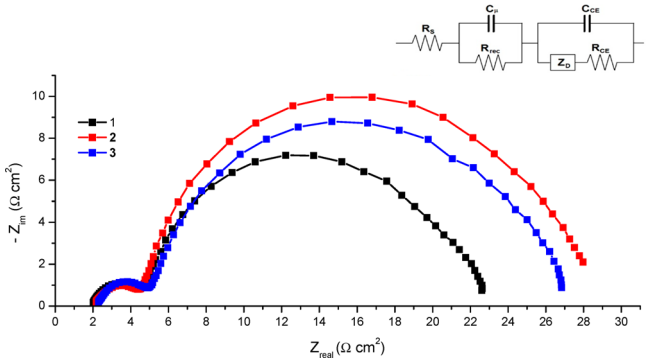


**Figure 8.** Electrochemical impedance spectroscopy (EIS) of DSSCs based on **1**−**3** as dyes.

imaginary part of the impedance is plotted as a function of the real part over the range of frequencies. Under soft illumination, at open circuit voltage conditions, the properties of the sensitized $TiO_2$/electrolyte interface can be derived from the Nyquist plot in terms of recombination resistance ($R_{rec}$), which has been obtained from the width of the main arc and by fitting the data with the equivalent circuit reported in the inset of Figure 8. Dyes **1**−**3** show similar recombination resistances (Table 4), so that the influence, on the dark current, of the

**Table 4. Recombination Resistance Calculated from EIS Plots of DSSC Based on Dyes 1−3**

| dye | $R_{rec}$ (Ω cm²) |
|---|---|
| **1** | 18 |
| **2** | 24 |
| **3** | 22 |

nature of the bridge between the porphyrinic core and the $\pi$ delocalized substituent in the $\beta$ position, does not appear to be significant.

## CONCLUSIONS

In this work, inspired by a previous investigation of Bisquert, Langa et al.,[9] we have successfully obtained and investigated three novel $Zn^{II}$ porphyriniates (**1**−**3**), for applications as sensitizers in DSSCs. These dyes consist of a combination of a porphyrinic core and a thiophenic $\pi$ delocalized chain. In particular the ability of the thiophenic DTE unit to significantly absorb in the region 430−650 nm has been exploited when this unit, bearing a cyanoacrylic anchoring group, is linked in the $\beta$ position to the porphyrinic core by 4-ethynylstyryl (**1**), ethynyl (**2**), and ethenyl (**3**) bridges.

As reported by Bisquert, Langa et al.[9] for a $Zn^{II}$-porphyrinic dye substituted in the *meso* position by a thiophenic $\pi$ delocalized chain, the increased elongation of the $\pi$ chain in the $\beta$ position, by adding a DTE unit, produces a panchromatic effect, as confirmed by the electronic absorption and IPCE spectra of **1**−**3**. In these IPCE spectra, the presence of a $\pi$ chain containing the thiophenic DTE unit conferred an electronic absorption spectrum covering a wide wavelengths range, as reflected in the broad plateau in the region 430−650 nm. However some significant differences are noteworthy in comparing the IPCE spectra of these dyes. Although they have, as in the case of **2** and **3**, quite similar light harvesting capability, they differ in terms of spatial structure due to the different nature of the bridge, which is ethenylic for **3** and ethynylic for **2**.

Consequently, while dyes **1** and **2** show a quite constant intensity of IPCE plateau of about 60%, similar to that reported for the *meso* analogous investigated by Bisquert, Langa et al.[9] dye **3** exhibits a significantly lower intensity (about 40%) of the IPCE plateau which translated in a lower solar cell efficiency ($\eta$ = 4.3%) with respect to **1** ($\eta$ = 5.2%) and **2** ($\eta$ = 4.7%). This difference is mainly due to a decrease in the photocurrent of the DSSC based dye **3**. A DFT theoretical investigation was conducted on an interaction model of porphyrinic dyes **2** and **3** with the $TiO_2$ surface, consisting of each dye anchored to a cluster of 82 $TiO_2$ units. The investigation has suggested a slightly lower quantum yield of electron injection into the $TiO_2$ semiconductor for **3** when compared to **2**, due to a smaller overlap between the LUMO orbital of the dye and the $TiO_2$ conduction band. As a consequence these calculations suggest an easier electron injection from the excited state of dye **2** when compared to dye **3**. It appears that this difference is dependent on the relative spatial positioning of the thiophenic $\pi$ chain and the porphyrinic core in the structure of the dye. The more extended ethynylstyryl bridge of **1** and even the ethynyl bridge of **2** are characterized by a significant planarity and linearity of the structure of dye **1** and at a lower extent of dye **2** to be compared with the crowded and more distorted structure of dye **3**. This linearity may favor an enhanced charge separation which could improve the electron injection process and charge transfer into the $TiO_2$ semiconductor. It appears thus that the increased conjugation between the porphyrinic core and the $\pi$ thiophenic chain in the $\beta$ position suggested by the lower HOMO−LUMO band gap of **3** when compared to **2** does not play a significant role.

In conclusion our work has shown that the panchromatic strategy, developed by Bisquert, Langa et al.,[9] may also be applied when the thiophenic $\pi$ chain containing a DTE unit is linked in the $\beta$ position to the porphyrinic ring. In addition we have clearly demonstrated that the efficiency of the DSSC based on these new dyes is dependent on the nature of the bridge between the DTE unit and the porphyrinic core, which influences the overall structural arrangement and consequently the charge separation involved in the electron injection process.

## ASSOCIATED CONTENT

### Supporting Information

Full description of the material. This material is available free of charge via the Internet at http://pubs.acs.org.


dx.doi.org/10.1021/jp412087f | J. Phys. Chem. C 2014, 118, 7307−7320

## AUTHOR INFORMATION


### Corresponding Author

*Phone: ++39-0250314363. E-mail: maddalena.pizzotti@unimi.it.


### Notes

The authors declare no competing financial interest.

## ACKNOWLEDGMENTS

M. Pizzotti and G. di Carlo thank the Fondazione Tronchetti Provera for financial support. A. Amat and F. De Angelis thank CNR-EFOR and CNR-RADIUS and EU Research Projects for financial support through FP7-NMP-2009 project 246124 "SANS". We thank Prof. Renato Ugo for useful discussions.

## REFERENCES


(1) (a) O'Regan, B.; Grätzel, M. A Low-Cost, High-Efficiency Solar Cell Based on Dye-Sensitized Colloidal Titanium Dioxide Films. *Nature* **1991**, *353*, 737−740. (b) Hagfeldt, A.; Grätzel, M. Light-Induced Redox Reactions in Nanocrystalline Systems. *Chem. Rev.* **1995**, *95*, 49−68. (c) Grätzel, M. Photoelectrochemical Cells. *Nature* **2001**, *414*, 338−344. (d) Grätzel, M. Mesoscopic Solar Cells for Electricity and Hydrogen Production from Sunlight. *Chem. Lett.* **2005**, *34*, 8−13.

(2) Robertson, N. Optimizing Dyes for Dye-Sensitized Solar Cells. *Angew. Chem., Int. Ed.* **2006**, *45*, 2338−2345.

(3) Hasobe, T.; Imahori, H.; Kamat, P. V.; Ahn, T. K.; Kim, S. K.; Kim, D.; Fujimoto, A.; Hirakawa, T.; Fukuzumi, S. Photovoltaic Cells Using Composite Nanoclusters of Porphyrins and Fullerenes with Gold Nanoparticles. *J. Am. Chem. Soc.* **2005**, *127*, 1216−1228.

(4) Li, L. L.; Diau, E. W. G. Porphyrin-Sensitized Solar Cells. *Chem. Soc. Rev.* **2013**, *42*, 291−304.

(5) Yella, A.; Lee, H. W.; Tsao, H. N.; Yi, C.; Chandiran, A. K.; Nazeeruddin, M. K.; Diau, E. W. G.; Yeh, C. Y.; Zakeeruddin, S. M.; Grätzel, M. Porphyrin-Sensitized Solar Cells with Cobalt (II/III)-Based Redox Electrolyte Exceed 12% Efficiency. *Science* **2011**, *334*, 629−634.

(6) (a) Lo, C. F.; Hsu, S. J.; Wang, C. L.; Cheng, Y. H.; Lu, H. P.; Diau, E. W. G.; Lin, C. Y. Tuning Spectral and Electrochemical Properties of Porphyrin-Sensitized Solar Cells. *J. Phys. Chem. C* **2010**, *114*, 12018−12023. (b) Bessho, T.; Zakeeruddin, S. M.; Yeh, C. Y.; Diau, E. W. G.; Grätzel, M. Highly Efficient Mesoscopic Dye-Sensitized Solar Cells Based on Donor-Acceptor-Substituted Porphyrins. *Angew. Chem., Int. Ed.* **2010**, *49*, 6646−6649. (c) Chang, Y. C.; Wang, C. L.; Pan, T. Y.; Hong, S. H.; Lan, C. M.; Kuo, H. H.; Lo, C. F.; Hsu, H. Y.; Lin, C. Y.; Diau, E. W. G. A Strategy to Design Highly Efficient Porphyrin Sensitizers for Dye-Sensitized Solar Cells. *Chem.Commun.* **2011**, *47*, 8910−8912. (d) Wang, C. L.; Lan, C. M.; Hong, S. H.; Wang, Y. F.; Pan, T. Y.; Chang, C. W.; Kuo, H. H.; Kuo, M. Y.; Diau, E. W. G.; Lin, C. Y. Enveloping Porphyrins for Efficient Dye-Sensitized Solar Cells. *Energy Environ. Sci.* **2012**, *5*, 6933−6940.

(7) Orbelli Biroli, A.; Tessore, F.; Pizzotti, M.; Biaggi, C.; Ugo, R.; Caramori, S.; Aliprandi, A.; Bignozzi, C. A.; De Angelis, F.; Giorgi, G.; Licandro, E.; Longhi, E. A Multitechnique Physicochemical Investigation of Various Factors Controlling the Photoaction Spectra and of some Aspects of the Electron Transfer for a Series of Push-Pull Zn(II) Porphyrins Acting as Dyes in DSSCs. *J. Phys. Chem. C* **2011**, *115*, 23170−23182.

(8) Di Carlo, G.; Orbelli Biroli, A.; Pizzotti, M.; Tessore, F.; Trifiletti, V.; Acciarri, M.; Abbotto, A.; Amat, A.; De Angelis, F.; Mussini, P. M. Tetraaryl ZnII Porphyrinates Substituted at $\beta$-Pyrrolic Positions as Sensitizers in Dye-Sensitized Solar Cells: a Comparison with Meso-Disubstituted Push-Pull ZnII Porphyrinates. *Chem.—Eur. J.* **2013**, *19*, 10723−10740.

(9) Barea, E. M.; Caballero, R.; López-Arroyo, L.; Guerrero, A.; de la Cruz, P.; Langa, F.; Bisquert, J. Triplication of the Photocurrent in Dye Solar Cells by Increasing the Elongation of the $\pi$-Conjugation in Zn-Porphyrin Sensitizers. *ChemPhysChem* **2011**, *12*, 961−965.

(10) Ziessel, R.; Bauerle, P.; Ammann, M.; Barbieri, A.; Barigelletti, F. Exciton-like Energy Collection in an Oligothiophene Wire End-Capped by Ru- and Os-Polypyridine Chromophores. *Chem. Commun.* **2005**, 802−804.

(11) Jestin, I.; Frère, P.; Mercier, N.; Levillain, E.; Stievenard, D.; Roncali, J. Synthesis and Characterization of the Electronic and Electrochemical Properties of Thienylenevinylene Oligomers with Multinanometer Dimensions. *J. Am. Chem. Soc.* **1998**, *120*, 8150−8158.

(12) Oswald, F.; Islam, D. M. S.; Araki, Y.; Troiani, V.; de la Cruz, P.; Moreno, A.; Ito, O.; Langa, F. Synthesis and Photoinduced Intramolecular Processes of Fulleropyrrolidine-Oligothienylenevinylene-Ferrocene Triads. *Chem.—Eur. J.* **2007**, *13*, 3924−3933.

(13) Campbell, W. M.; Jolley, K. W.; Wagner, P.; Wagner, K.; Walsh, P. J.; Gordon, K. C.; Schmidt-Mende, L.; Nazeeruddin, M. K.; Wang, Q.; Grätzel, M.; Officer, D. L. Highly Efficient Porphyrin Sensitizers for Dye-Sensitized Solar Cells. *J. Phys. Chem. C* **2007**, *111*, 11760−11762.

(14) Frisch, M. J.; Trucks, G. W.; Schlegel, H. B.; Scuseria, G. E.; Robb, M. A.; Cheeseman, J. R.; Scalmani, G.; Barone, V.; Mennucci, B.; Petersson, G. A.; Nakatsuji, H.; Caricato, M.; Li, X.; Hratchian, H. P.; Izmaylov, A. F.; Bloino, J.; Zheng, G.; Sonnenberg, J. L.; Hada, M.; Ehara, M.; Toyota, K.; Fukuda, R.; Hasegawa, J.; Ishida, M.; Nakajima, T.; Honda, Y.; Kitao, O.; Nakai, H.; Vreven, T.; Montgomery, J. A., Jr.; Peralta, J. E.; Ogliaro, F.; Bearpark, M.; Heyd, J. J.; Brothers, E.; Kudin, K. N.; Staroverov, V. N.; Kobayashi, R.; Normand, J.; Raghavachari, K.; Rendell, A.; Burant, J. C.; Iyengar; S. S.; Tomasi, J.; Cossi, M.; Rega, N.; Millam, J. M.; Klene, M.; Knox, J. E.; Cross, J. B.; Bakken, V.; Adamo, C.; Jaramillo, J.; Gomperts, R.; Stratmann, R. E.; Yazyev; O.; Austin, A. J.; Cammi, R.; Pomelli, C.; Ochterski, J. W.; Martin, R. L.; Morokuma, K.; Zakrzewski, V. G.; Voth, G. A.; Salvador; P. ; Dannenberg; J. J.; Dapprich, S.; Daniels, A. D.; Farkas, Ö.; Foresman, J. B.; Ortiz, J. V.; Cioslowski, J.; Fox, D. J. *Gaussian 09 (Revision A.02)*; Gaussian, Inc.: Wallingford, CT, 2009.

(15) (a) Becke, A. D. Density-Functional Thermochemistry. III. The Role of Exact Exchange. *J. Chem. Phys.* **1993**, *98*, 5648−5652. (b) Lee, C.; Yang, W.; Parr, R. G. Development of the Colle-Salvetti Correlation-Energy Formula into a Functional of the Electron Density. *Phys. Rev. B* **1998**, *37*, 785−789. (c) Miehlich, B.; Savin, A.; Stoll, H.; Preuss, H. Results Obtained with the Correlation Energy Density Functionals of Becke and Lee, Yang and Parr. *Chem. Phys. Lett.* **1989**, *157*, 200−206.

(16) (a) McLean, A. D.; Chandler, G. S. Contracted Gaussian Basis Sets for Molecular Calculations. I. Second Row Atoms, Z = 11−18. *J. Chem. Phys.* **1980**, *72*, 5639−5648. (b) Krishnan, R.; Binkley, J. S.; Seeger, R.; Pople, J. A. Self-Consistent Molecular Orbital Methods. XX. A Basis Set for Correlated Wave Functions. *J. Chem. Phys.* **1980**, *72*, 650−654. (c) Curtiss, L. A.; McGrath, M. P.; Blaudeau, J. P.; Davis, N. E.; Binning, R. C., Jr.; Radom, L. Extension of Gaussian-2 Theory to Molecules Containing Third-Row Atoms Ga-Kr. *J. Chem. Phys.* **1995**, *103*, 6104−6113.

(17) Cossi, M.; Rega, N.; Scalmani, G.; Barone, V. Energies, Structures, and Electronic Properties of Molecules in Solution with the C-PCM Solvation Model. *J. Comput. Chem.* **2003**, *24*, 669−681.

(18) Yanai, T.; Tew, D.; Handy, N. A New Hybrid Exchange-Correlation Functional Using the Coulomb-Attenuating Method (CAM-B3LYP). *Chem. Phys. Lett.* **2004**, *393*, 51−57.

(19) De Angelis, F.; Fantacci, S.; Selloni, A. Alignment of the Dye's Molecular Levels with the $TiO_2$ Band Edges in Dye-Sensitized Solar Cells: a DFT-TDDFT Study. *Nanotechnology* **2008**, *19*, 424002−424007.

(20) (a) Anselmi, C.; Mosconi, E.; Pastore, M.; Ronca, E.; De Angelis, F. Adsorption of Organic Dyes on TiO2 Surfaces in Dye-Sensitized Solar Cells: Interplay of Theory and Experiment. *Phys. Chem. Chem. Phys.* **2012**, *14*, 15963−15974. (b) Pastore, M.; De Angelis, F. Computational Modelling of $TiO_2$ Surfaces Sensitized by Organic Dyes with Different Anchoring Groups: Adsorption Modes, Electronic Structure and Implication for Electron Injection/Recombination. *Phys. Chem. Chem. Phys.* **2012**, *14*, 920−928. (c) De Angelis,

F.; Fantacci, S.; Mosconi, E.; Nazeeruddin, M. K.; Grätzel, M. Absorption Spectra and Excited State Energy Levels of the N719 Dye on TiO2 in Dye-Sensitized Solar Cell Models. *J. Phys. Chem. C* **2011**, *115*, 8825−8831.
(21) Bard, A. J.; Faulkner, L. R. *Electrochemical Methods. Fundamentals and Applications*; Wiley: New York, 2002; pp 648−650.
(22) Gritzner, G.; Kuta, J. Recommendations on Reporting Electrode Potentials in Nonaqueous Solvents. *Pure Appl. Chem.* **1984**, *56*, 461−466.
(23) Gritzner, G. Polarographic Half-Wave Potentials of Cations in Nonaqueous Solvents. *Pure Appl. Chem.* **1990**, *62*, 1839−1858.
(24) Ito, S.; Murakami, T. N.; Comte, P.; Liska, P.; Grätzel, C.; Nazeeruddin, M. K.; Grätzel, M. Fabrication of Thin Film Dye Sensitized Solar Cells with Solar to Electric Power Conversion Efficiency over 10%. *Thin Solid Films* **2008**, *516*, 4613−4619.
(25) Gouterman, M.; Wagniere, G. H.; Snyder, L. C. Spectra of Porphyrins. II. Four-Orbital Model. *J. Mol. Spectrosc.* **1963**, *11*, 108−127.
(26) (a) Muscat, J. P.; Newns, D. M. Chemisorption on Metals. *Prog. Surf. Sci.* **1978**, *9*, 1−43. (b) Nilsing, M.; Persson, P.; Ojamäe, L. Anchor Group Influence on Molecule-Metal Oxide Interfaces: Periodic Hybrid DFT Study of Pyridine Bound to $TiO_2$ via Carboxylic and Phosphonic Acid. *Chem. Phys. Lett.* **2005**, *415* (4−6), 375−380.
(27) Amaya, T.; Shimizu, Y.; Yakushi, Y.; Nishina, Y.; Hirao, T. Transition Metal-Directed Self-Assembly of Porphyrins Bearing Redox-Active Phenylenediamine Pendant. *Tetrahedron Lett.* **2010**, *51*, 2416−2419.
(28) Mussini, P. R.; Orbelli Biroli, A.; Tessore, F.; Pizzotti, M.; Biaggi, C.; Di Carlo, G.; Lobello, M. G.; De Angelis, F. Modulating the Electronic Properties of Asymmetric Push-Pull and Symmetric Zn(II)-Diarylporphyrinates with Para Substituted Phenylethynyl Moieties in 5,15 Meso Positions: A Combined Electrochemical and Spectroscopic Investigation. *Electrochim. Acta* **2012**, *85*, 509−523.
(29) Kadish, K. M.; Caemelbecke, E. V. Electrochemistry of Porphyrins and Related Macrocycles. *J. Solid State Electrochem.* **2003**, *7*, 254−258.
(30) Zerner, M.; Gouterman, M. Porphyrins. IV. Extended Hueckel Calculations on Transition Metal Complexes. *Theor. Chim. Acta* **1966**, *4*, 44−63.
(31) Bolzoni, A.; Baldoli, C.; Bossi, A.; Licandro, E.; Maiorana, S.; Viglianti, L.; Mussini, P. R. Synthesis, Photophysics, and Electrochemistry of Tetra(2-thienyl)ethylene (TTE) Derivatives. *Eur. J. Org. Chem.* **2013**, 7489−7499.
(32) Noviandri, I.; Brown, K. N.; Fleming, D. S.; Gulyas, P. T.; Lay, P. A.; Maasters, A. F.; Phillips, L. The Decamethylferrocenium/Decamethylferrocene Redox Couple: A Superior Redox Standard to the Ferrocenium/Ferrocene Redox Couple for Studying Solvent Effects on the Thermodynamics of Electron Transfer. *J. Phys. Chem. B* **1999**, *103*, 6713−6722.
(33) Bard, A. J.; Faulkner, L. R. *Electrochemical Methods. Fundamentals and Applications*; II ed.; Wiley: New York, 2001; pp 505−509.
(34) Heinze, J.; Frontana-Uribe, B. A.; Ludwigs, S. Electrochemistry of Conducting Polymers-Persistent Models and New Concepts. *Chem. Rev.* **2010**, *110* (8), 4724−4771.
(35) Longhi, E.; Bossi, A.; Di Carlo, G.; Maiorana, S.; De Angelis, F.; Salvatori, S.; Petrozza, A.; Binda, M.; Roiati, V.; Mussini, P. R.; Baldoli, C.; Licandro, E. Metal-Free Benzodithiophene-Containing Organic Dyes for Dye-Sensitized Solar Cells. *Eur. J. Org. Chem.* **2013**, 84−94.
(36) Pastore, M.; Fantacci, S.; De Angelis, F. Ab Initio Determination of Ground and Excited State Oxidation Potentials of Organic Chromophores for Dye-Sensitized Solar Cells. *J. Phys. Chem. C* **2010**, *114*, 22742−22750.